Journal Name

ARTICLE TYPE

Cite this: DOI: 10.1039/xxxxxxxxxx

Geometrical and energetical structural changes in organic dyes for dye-sensitized solar cells probed with photoelectron spectroscopy and DFT

Susanna K. Eriksson,[a] Ida Josefsson,[b] Hanna Ellis,[a] Anna Amat,[c] Mariachiara Pastore,[c] Johan Oscarsson,[d] Rebecka Lindblad,[d] Erik M. J. Johansson,[a] Gerrit Boschloo,[a] Anders Hagfeldt,[e] Simona Fantacci,[c] Michael Odelius,*[b] and Håkan Rensmo*[d]

Received Date
Accepted Date

DOI: 10.1039/xxxxxxxxxx

www.rsc.org/journalname

The effects from alkoxy chain length in triarylamine based donor-acceptor organic dyes are investigated with respect to the electronic and molecular surface structure and the effect on solar cell performance and electron lifetime. The dyes were investigated when adsorbed on the TiO_2 in a configuration that can be used in dye-sensitized solar cells (DSCs). Specifically, the two dyes D35 and D45 were compared using photoelectron spectroscopy (PES) and density functional theory (DFT) calculations. The differences in solar cell characteristics when longer alkoxy chains are introduced in the dye donor unit are attributed to geometrical changes in the dye packing while only minor differences were observed in the electronic structure. A higher dye load was observed for D45 on TiO_2. However, D35 based solar cells result in higher photocurrent although the dye load is lower. This is explained by the different geometrical structures of the dyes on the surface.

1 Introduction

Dye-sensitized solar cells (DSCs) showed a breakthrough with the report in the early 1990's by Grätzel and O'Regan[1] and is currently a research area with great potential.[2] The benefit is the possibility to harvest sunlight for energy production at low cost. Since the earliest publications, a lot of efforts have been made to fully understand the complicated nature of these nano structured solar cells. The basic principle is to use a dye molecule that absorbs sunlight. The dye is attached to a semiconductor (usually TiO_2) and a liquid electrolyte or solid hole transporter is used to regenerate the dye after electron injection into the semiconductor.

During recent years a new family of organic dyes containing the triarylamine unit has been developed and functionalized for different purposes.[3–7] When D35 (see Figure 1) was introduced as new sensitizer for DSCs together with the new redox couple based on cobalt complexes, the steric hindrance for recombination was of great importance.[8] In a previous paper[9], we also report on how the linker unit in the dye molecule will affect the solar cell performance and also the adsorption configurations and coverage. Another recent paper states that steric hindrance will lead to a blocking effect and therefore longer electron lifetime.[10]

In the present paper we investigate how the length of the alkoxy groups on the triarylamine unit affects the electron lifetime by comparing two dyes where one contains longer alkane

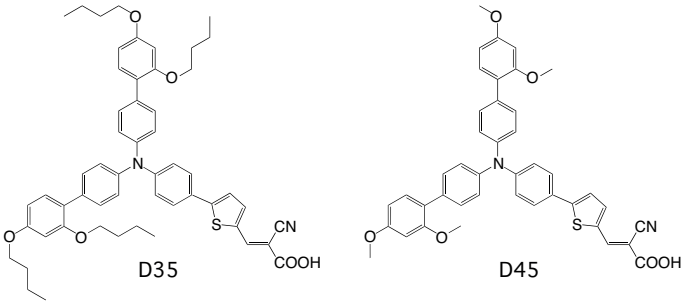

Fig. 1 Structure of the dye molecules D35 and D45.

[a] Department of Chemistry-Ångström, Uppsala University, Box 523, SE-751 20 Uppsala, Sweden
[b] Department of Physics, Stockholm University, AlbaNova University Center, SE-106 91 Stockholm, Sweden. E-mail: odelius@fysik.su.se
[c] Istituto CNR di Scienze e Tecnologie Molecolari (CNR-ISTM), Computational Laboratory for Hybrid/Organic Photovoltaics (CLHYO), via Elce di Sotto 8, I-06123 Perugia, Italy.
[d] Department of Physics and Astronomy, Uppsala University, Box 516, SE-751 20 Uppsala, Sweden. Fax: +46 18 471 5999; Tel: +46 18 471 3547; E-mail: hakan.rensmo@physics.uu.se
[e] Laboratory of Photomolecular Science, Institute of Chemical Sciences and Engineering, School of Basic Sciences, Ecole Polytechnique Fédérale de Lausanne (EPFL), CH-1015 Lausanne, Switzerland.

chains (see molecular structures in Figure 1). While D35 has o,p-dibutoxyphenyl units attached to the triarylamine unit, D45 [11] has o,p-dimetoxyphenyl units. D35 and D45 are both organic dyes with donor-linker-acceptor structure. The donor part consists of the triarylamine unit, including the alkoxy chains, where the nitrogen possesses most of the positive charge upon oxidation. [12,13] The linker unit in both cases is a thiophene, being conjugated in order to facilitate the electron transfer from donor to acceptor. The acceptor is the cyanoacrylic acid, which binds to the TiO_2, and from which the electron is injected into the semiconductor.

These two dyes are investigated by photoelectron spectroscopy (PES) and density functional theory (DFT) both concerning adsorption configurations on the surface and calculations in gas phase to probe the energy levels. The findings of PES and DFT are also complemented by solar cell data.

2 Methods

2.1 Solar cell preparation and characterization

The solar cells were prepared using a standard method reported before. [9] In short the method is as follows. Fluorine doped tin oxide glass substrates (Pilkington, TEC 15) were treated with 40 mM aqueous $TiCl_4$ solution. The TiO_2 films were screen printed with one absorption layer (Dyesol DSL 30 NR-D) and one scattering layer (Dyesol WER2-O) to a total thickness of about 7.5 μm. After the screen printing the samples were stepwize heat treated up to 500 °C (60 min). After the sintering the samples were treated in aqueous $TiCl_4$ solution again and rinsed. A final heating step (500 °C for 60 min) was performed after the $TiCl_4$ treatment. The dye baths had a concentration of 0.2 mM D35 or D45 in ethanol. The organic D35 and D45 dyes were synthesized by published procedures. [4,11] The electrodes were sensitized for 16 hours before solar cell assembly. For the counter electrode, TEC8 was used and a platinum catalyst was deposited. The electrolyte contained 0.22 M $Co[(bpy)_3](PF_6)_2$, 0.05 M $Co[(bpy)_3](PF)_3$, 0.2 M 4-*tert*-butylpyridine (TBP) and 0.1 M $LiClO_4$ in acetonitrile.

Current-voltage (IV) measurements were carried out with a Keithley 2400 source and a Newport solar simulator (model 91160). Light intensity was calibrated, using a certified reference solar cell (Fraunhofer ISE), to an intensity of 1000 W m^{-2} (1 sun). For the IV-measurements a black mask of 0.4×0.4 cm^2 was used in order to avoid significant additional contribution from light falling on the device outside the active area (0.5×0.5 cm^2). Electron lifetime measurements were carried out using a white LED (Luxeon Star 1 W) as light source. Voltage and current were monitored by a 16-bit resolution digital acquisition board (National Instruments) in combination with a current amplifier (Stanford Research Systems SR570) and a custom made system using electromagnetic switches. The electron lifetimes were determined by monitoring the transient photovoltage at different light intensities when applying a small (10 mV) square wave modulation to the bias of the LED. The resulting photovoltaic transients were fitted using first order kinetics to obtain time constants. IV measurements and electron lifetime measurements were performed on the same day as the assembly of the solar cells.

Incident photon to current conversion efficiency (IPCE) spectra were recorded using a computer controlled setup consisting of a xenon light source (Spectral Products ASB-XE-175), a monochromator (Spectral Products CM110) and a potentiostat (EG&G PAR 273). Calibration was performed using a certified reference solar cell (Fraunhofer ISE). The IPCE measurements were carried out 48 hours after assembly of the solar cells.

2.2 Photoelectron spectroscopy

The samples for photoelectron spectroscopy (PES) measurements were prepared by using similar working electrodes as for the solar cell preparation, with the difference that the paste used was DSL 18 NR-T (purchased from Dyesol) and the scattering layer and the $TiCl_4$ post treatment were excluded. The electrodes were sensitized for 15-16 h and transferred to the vacuum system immediately after sensitization. The PES measurements were performed using synchrotron radiation at BL I411 at the Swedish national laboratory MAX IV in Lund. [14] The electron take off angle was 60 ° and the electron take off direction was collinear with the e-vector of the incident photon beam, i.e. the analyzer was placed orthogonal to the incoming photons. The kinetic energies of the photoelectrons were measured using a Scienta R4000WAL analyzer. The PES spectra were binding energy calibrated by setting the $Ti2p_{3/2}$ substrate signal to 458.56 eV. [15] The techniques are described elsewhere in more detail. [15,16] When using PES the inelastic mean free path (IMFP) of the emitted electrons depends on their kinetic energy. Therefore measurements with lower photon energy will be more surface sensitive compared to measurements with higher photon energy.

The experimental X-ray absorption spectra (XAS) were also measured at beamline I411. N1s XAS spectra were recorded by detection of secondary electrons in partial yield mode and intensity normalized versus the number of incident photons. The photon energy calibration was performed by detecting Ti3p from the substrate using first and second order light.

2.3 Theoretical modeling

2.3.1 Adsorption configuration calculations.

Different adsorption geometries of D35 and D45 onto the TiO_2 anatase (101) surface were investigated using density functional theory (DFT) methods. The interacting dye at TiO_2 system is composed of the D35 (D45) dye and a neutral stoichiometric $(TiO_2)_{82}$ cluster of nanometric dimension, obtained by appropriately cutting an anatase slab exposing the majority (101) surface. [17,18] Based on insights gained from previous extensive investigations, we here only consider configurations of the dye molecules interacting with the TiO_2 surface via the bidentate anchoring carboxylate group, by transfer of a proton to an oxygen atom vicinal to the adsorption site. [19–23] Two different bidentate adsorption configurations, which differ in the orientation of the dye with respect to the surface, were evaluated: (i) the dye is standing on the TiO_2 surface; (ii) the sensitizer is bent on the semiconductor surface (smaller binding angle). The two configurations are hereafter referred to as "up" and "flat", respectively. The considered dye@TiO_2 systems were optimized by the means

of the ADF code[24,25] employing the PBE exchange-correlation functional[26] corrected for the dispersion.[27] A DZ basis set for all the Ti and O atoms of the TiO_2 cluster and a DZP basis set for all the C, N, O and H atoms of the dyes were utilized.[28] On the optimized bidentate adsorption geometries we carried out single point calculations with PBE exchange-correlation functional including solvation effects by means of a conductor-like screen model (COSMO)[29–31] as implemented in the ADF code.[32] Ethanol was employed as solvent, thus assigning the ADF default values to the dielectric constant (24.55) and to the radius (2.85 Å) of solvent rigid spheres.

2.3.2 Spectrum calculations.

Spectrum calculations were performed on the isolated D35 and D45 molecules using DFT. The geometry optimization and photoelectron calculations were performed using the StoBe-deMon code[33] with pure gradient corrected density functionals[34,35] and double-zeta valence basis sets including polarization functions.[36] For comparison to the experimental valence photoemission spectra, we derived the density of states (DOS) from electronic ground state calculations. The contribution to the total spectrum from the different units was investigated through a decomposition of the total DOS into partial DOS (PDOS) by projection onto groups of N, C, O, and S atoms in a Löwdin analysis. Direct comparison to experimental spectra was done by adding a constant shift of -3.0 eV to all calculated DOS curves. A Gaussian broadening of 0.5 eV full-width at half-maximum was used for comparison of the calculated PDOS to the experimental data.

In the XAS simulations, the half-core hole transition potential approximation[37] within DFT was employed, and for an accurate description of the core-excited nitrogen atom we used the IGLO-III basis set.[38] Localization of the core-hole was ensured by treating the remaining nitrogen atom with an effective core potential in combination with the O-NITROGEN(+5) (211/21) basis set.[39,40] The XAS spectrum was generated in a double base set procedure,[41] and for comparison to experiment broadened with a Gaussian function of 0.6 eV full-width at half-maximum. The TZVP basis set was used to all other atoms,[42] and the DFT functional was approximated by the same correlation functional,[34,35] as for the density of states.

For the PDOS and XAS calculations, the auxilary basis sets were generated using the GENA3 option in StoBe-deMon code,[33] except for the nitrogen ECP on which a (5,2;5,2) basis set was employed.

3 Results and discussion

3.1 Solar cell characteristics

In Figure 2 the IV characteristics of D35 and D45 based solar cells are shown. The values from the IV measurements are summarized in Table 1 and it can be seen that D35 gives higher V_{OC} and J_{SC} compared to D45. Three solar cells of each dye were assembled and master solar cell results are presented.

The incident photon to current conversion efficiency (IPCE) curves for the solar cells based on the two different dyes are very similar as shown in Figure 3. When measuring IPCE, lower light intensities are used compared to the IV-measurements, where 1 sun is used. The lower light intensity used when measuring IPCE causes a difference when comparing the J_{SC} and the integrated current of the IPCE. The integrated current obtained from the IPCE measurements are slightly lower than the J_{SC} for both dyes. The integrated currents for D35 and D45 were 7.9 $mAcm^{-2}$ and 7.4 $mAcm^{-2}$, respectively. However, the trend is the same with the integrated currents as with the J_{SC} values, D35 based solar cells show somewhat higher current values.

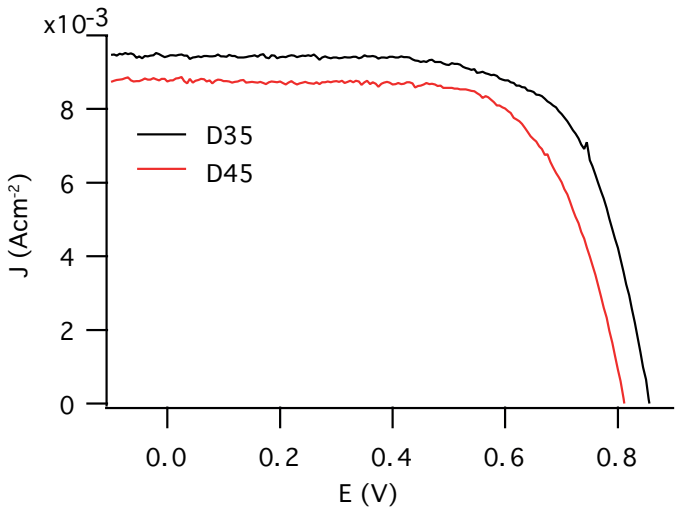

Fig. 2 Current-voltage (IV) curves for D35 and D45 -sensitized solar cells with cobalt-based electrolyte under 100 mW cm^{-2} AM1.5G illumination.

Table 1 Summary of solar cell characteristics. V_{OC} is the open circuit voltage, J_{SC} is the short circuit current, FF is the fill factor and η is the overall power conversion efficiency

Dye	V_{OC} (V)	J_{SC} (mA/cm^2)	FF	η (%)
D35	0.86	9.43	0.69	5.6
D45	0.81	8.8	0.68	4.8

The V_{OC} differs for the solar cells assembled with D35 and D45 dye molecules, and D35 based solar cells obtain a higher V_{OC} by 50 mV compared to the D45 equivalents. Moreover, D35 has earlier been shown to work well in cobalt redox mediator systems, partly explained by preventing close contact between the oxidized species in the electrolyte and the TiO_2 surface.[8] The V_{OC} of a dye-sensitized solar cell generally arise from the difference between the *quasi*-Fermi level for electrons in the TiO_2 and the redox potential of the redox mediator. Since the solar cells investigated here are assembled with the same electrolyte, the *quasi*-Fermi level of TiO_2 determines the V_{OC}. The *quasi*-Fermi level is ultimately limited by the position of the conduction band edge of TiO_2, which can be assumed to be the same for these two dyes.[9,43] The V_{OC} difference for the two dyes may therefore be largely dependent on the electron lifetime, the time the electron stays in the TiO_2 before recombining to the oxidized species in the electrolyte or to the oxidized dye. The electron lifetime was measured and the curves are displayed in Figure 4.

By the electron lifetime measurements, there is a clear difference shown for the two different dyes. D35 renders much longer

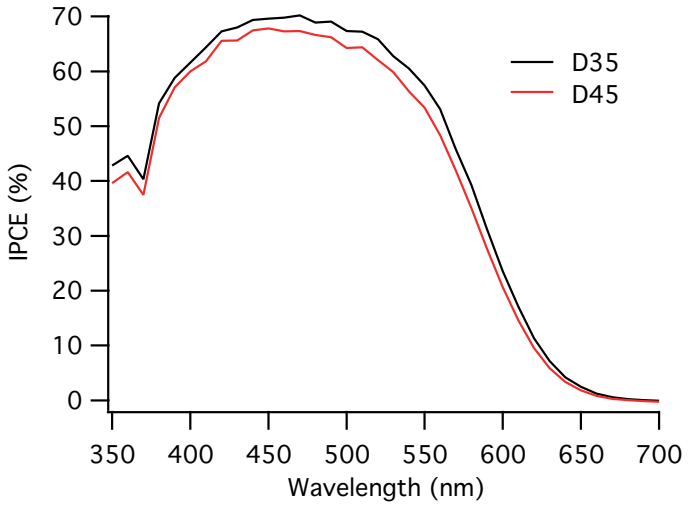

Fig. 3 Incident photon to current conversion efficiency (IPCE) for D35 and D45-sensitized solar cells.

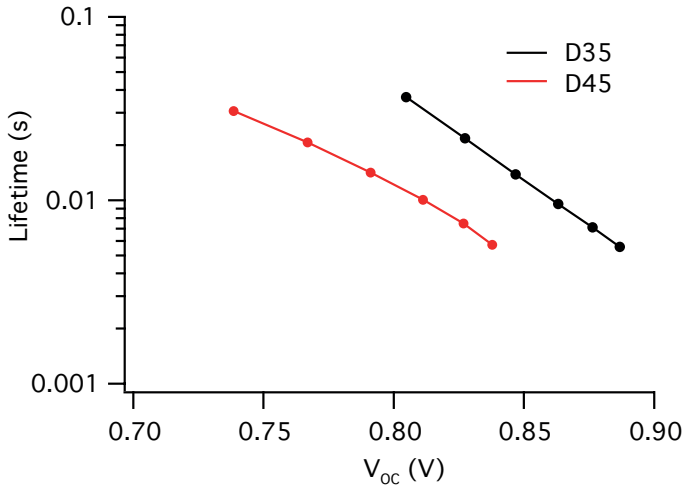

Fig. 4 Electron lifetimes in D35 and D45 dye-sensitized solar cell systems where D35 based solar cells clearly render longer electron lifetimes.

electron lifetimes compared to D45.In a previous study it was also shown that the recombination rate for D35 was longer also when the surface coverage was taken into account.[44] As partly highlighted above, there are two plausible explanations for the differences in solar cell performance; geometrical or energetical. PES measurements and DFT calculations were conducted to obtain a detailed understanding of the differences at an atomic level. The results are reported in the following sections.

3.2 Geometrical configurations

To shed some light on the difference in solar cell performance and especially the significant difference in electron lifetimes, the geometrical configurations were investigated both experimentally using PES and theoretically by DFT calculations. To investigate the adsorption geometries of the D35 and D45 sensitizers and the chemical bonding to the TiO_2 substrate, DFT calculations of an adsorption model, in which the adsorbate and substrate are explicitly included in DFT calculations and the solvent (ethanol) is implicitly represented, were performed. The calculations also facilitate an interpretation of the spectral data from the PES experiments.

According to our calculations in ethanol solution, the most stable adsorption geometry is the one obtained with the dye standing up, by ca. 17 kcal/mol (0.7 eV), for both D35 and D45. A stabilization of the "flat" adsorption mode was found in vacuo, likely due to the unscreened interaction with TiO_2 surface. As a matter of fact, in vacuo the "up" geometry is only ca. 3 (2) kcal/mol more stable than the "flat" one for D35 (D45). In Figure 5 the "up" and "flat" configurations are reported for D35 and D45 along with the main geometrical parameters related to the interaction between the dye and the TiO_2 surface. Noticeably, the longer alkoxy chains do not affect the adsorption geometry, at least in a static picture. In fact, the geometrical parameters are similar for D35 and D45.

The maximum surface packing of the adsorbed dyes in their most stable "up" configuration, (avoiding explicit superposition among the dye atoms) was simulated and is illustrated in Figure 6. A larger packing density was found for D45 compared to D35, with D45 providing a 47 % higher maximum coverage, which can be seen as an upper limit in ideal conditions.

Using PES, the dye coverage can be estimated by a comparison of the intensity of the S2p core-level signals normalized versus the corresponding Ti2p (substrate) signals. As seen in the S2p spectra presented in Figure 7, the coverage of D45 on the surface is significantly higher in relation to D35. The relative intensities for S2p vs. Ti2p are 1 (D35) and 1.3 (D45). A conclusion from the analysis of the S2p core-level spectra is that there are approximately 30 % more dye molecules at the surface with D45 as compared to D35. This value is in line with the larger coverage obtained from DFT calculations for D45. The difference in coverage is directly linked to the larger size of D35 due to the longer alkoxy chains.

To gain experimental insight into the adsorption at the TiO_2 surface and orientation of the adsorbed dye molecules, the N1s core-level photoelectron spectra were measured using different photon energies of the ionizing light. D35 and D45 contain two chemically different nitrogen atoms, in a cyano (acceptor) group,

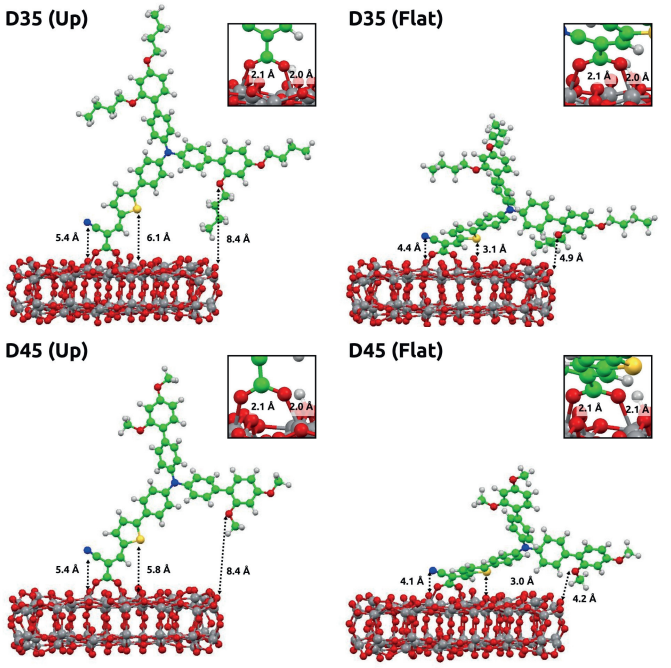

Fig. 5 Binding configurations for D35 and D45 with one "up" (standing) and one "flat" (smaller binding angle) mode.

from now denoted as N_A, and in a triarylamine group (donor), from now denoted as N_D. Since the covalent bonding around these nitrogen atoms is only weakly affected by elongation of the alkoxy groups, differences in N1s core-level spectra can be assigned predominantly to differences in adsorption geometry. The core-level peaks originating from these two different nitrogen atoms have different binding energies and can be separated by peak fitting, see Figure 8. By comparing the intensities for the different nitrogen (N1s) contributions a signal ratio can be estimated, *i.e.* how much of the total signal originates from each nitrogen. Since PES is highly surface sensitive and the intensity is proportional to the inelastic mean free path (IMFP) of the photoelectrons, the average distance (perpendicular to the outermost surface) between the nitrogen atoms in the molecule on the TiO_2 surface can be estimated.

A smaller difference in distance to the open surface reflects a smaller binding angle and vice versa. The higher the energy of the photons, the higher the kinetic energy of the electrons and consequently the longer the inelastic mean free path (IMFP). As seen in the spectra, the N_A-contribution is decreasing with decreasing photon energy which is a consequence of the cyano groups being closer to the TiO_2 surface compared to the triarylamine groups. Hence, the dyes are standing on the surface with the triarylamine groups pointing out. By assuming a flat surface and normal emission, a more detailed value representing the molecular organization can be calculated using Equation 1 where I is the ratio between the N1s intensity from N_A and the total N1s intensity (N_{TOT}), λ is the inelastic mean free path and d is the average distance between the nitrogen atoms. Here $\lambda = 6$ Å for a photon energy of 540 eV and $\lambda = 8$ Å for a photon energy of 758 eV were used.[9,45,46] Using this procedure, the distance between

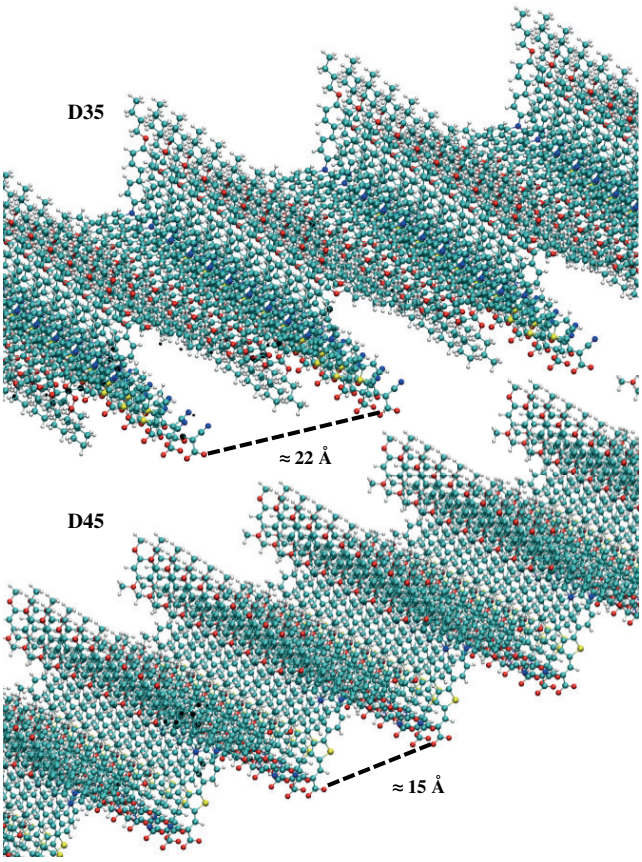

Fig. 6 Calculated packing density for D35 and D45. The closest packing possible is calculated avoiding repulsive overlap of atoms from the dye molecules. The maximum packing density for D45 is calculated to be approximately 47 % higher than for D35 on a TiO_2-surface.

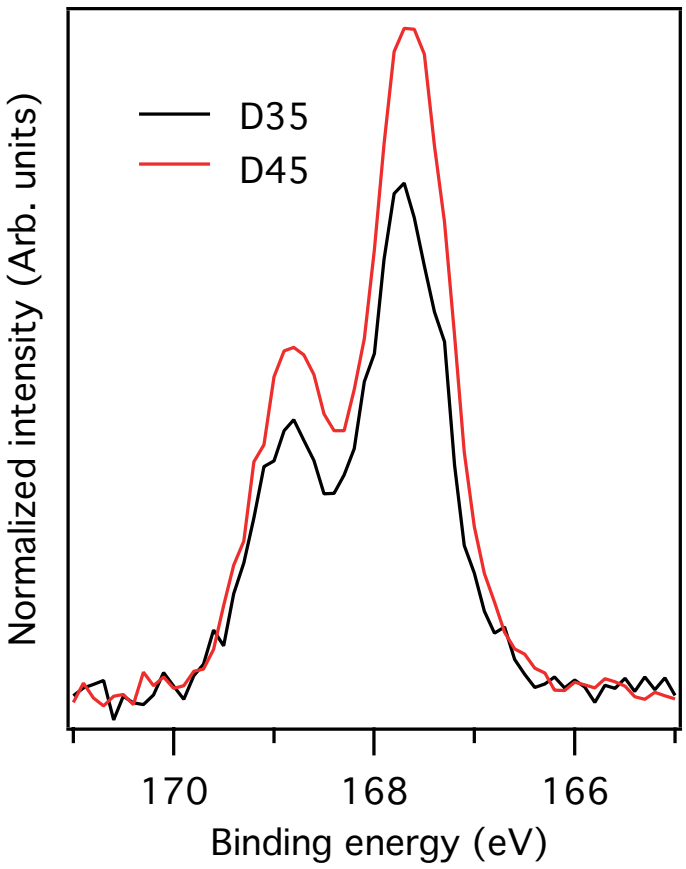

Fig. 7 The S2p core-level photoelectron spectra for D35 and D45. The spectra are measured with a photon energy of 758 eV and are intensity normalized versus the Ti2p signal. The intensities give a measure on the surface dye coverage.

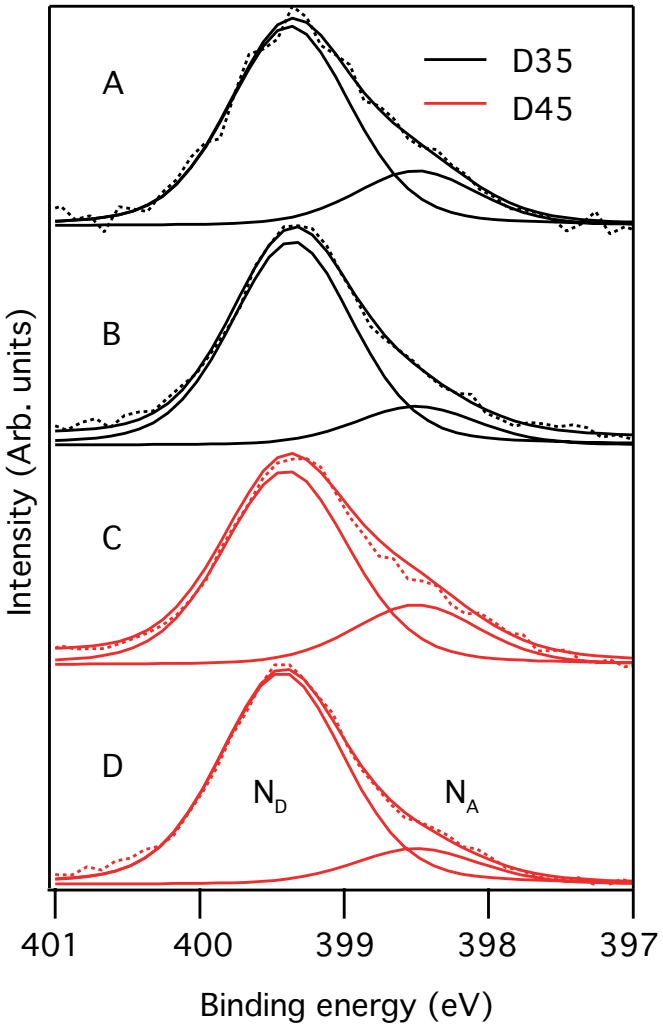

Fig. 8 Photon energy dependence in the N1s core-level photoelectron spectra, in which A and B are D35 while C and D are D45. A and C are measured with a photon energy of 758 eV and B and D with 540 eV. The lower the photon energy, the more surface sensitive are the measurements. The peaks at higher binding energy stem from the triarylamine unit (donor unit denoted N_D) and the smaller peaks at lower binding energy are from the CN-unit in the group bound to the surface (acceptor unit denoted N_A).

the two nitrogens projected onto the probing depth vector, *i.e.* in the probing direction, is 10 Å and 9 Å for D35 and D45, respectively. Considering the crudeness of this analysis, we conclude that the results for the two dyes are similar, hence the binding angle will be similar, a result which also is supported by the DFT calculations.

$$\frac{I}{I^0} = e^{-\frac{d}{\lambda}}, \quad (1)$$

In Figure 9, C1s core-level photoemission spectra measured with different photon energies are presented. It is important to note that D35 contains almost 30 % more carbon and therefore the signal should be 30 % more intense if all other parameters are fixed. On the other hand, we have showed above (experimentally and theoretically) that there are 30-47 % more dye molecules on the surface in the case of D45. Taking the total amount of carbon atoms on each sample into consideration, the C1s signal from D35 and D45 should therefore be similar in intensity. The broadening of the D45 C1s spectra at higher binding energies are due to the methoxy carbons only found in D45. At higher photon energy, *i.e.* less surface sensitive measurements, the intensities are also approximately the same. However, when probed with lower photon energy (454 eV), the C1s signal from D35 is 29 % stronger. At this low photon energy the outermost part of the surface is predominantly probed. Since the main difference between the dyes is the length of the alkoxy chains, this result indicates that the carbon-rich butoxy chains in D35 are located at the very top of the sample. The butoxy chains might form an entangled alkoxy layer that can prevent the electrons injected into the TiO_2 from recombining with the Co^{3+} complexes in the electrolyte. The cobalt based electrolyte will in its +2 state donate an electron to the oxidized dye and form a +3 state. These complexes will then be regenerated at the counter electrode. However, the unpreferred recombination reaction with injected electrons may also occur.

Table 2 Summary of the intensity ratios obtained from the PES measurements. The S2p signal is normalized versus the Ti2p signal and the D35 intensity. For N1s the ratio in intensity of the cyano nitrogen (acceptor) to the total intensity (N_A/N_{TOT}) is presented. The N-N distance d is estimated from Equation 1. The C1s spectra are normalized versus the corresponding Ti2p or Ti3p signal.

Dye	S2p	N1s 758eV	N1s 540eV	d	C1s 758eV	C1s 454eV
D35	1.0	0.23	0.15	10Å	5.5	59.3
D45	1.3	0.20	0.14	9Å	5.4	42

All intensity ratios are presented in Table 2. As a summary from the geometrical discussion we conclude that the introduction of longer alkoxy chains in the D35 dye leads to lower dye coverage but the binding orientation remains unaffected. As indicated by Figure 9, the alkoxy chains are pointing away from the TiO_2 surface and this can prevent the electrons injected into the TiO_2 from recombining with the electrolyte. The longer lifetime seen for D35 indicates that the longer alkoxy chains prevent recombination more efficiently.

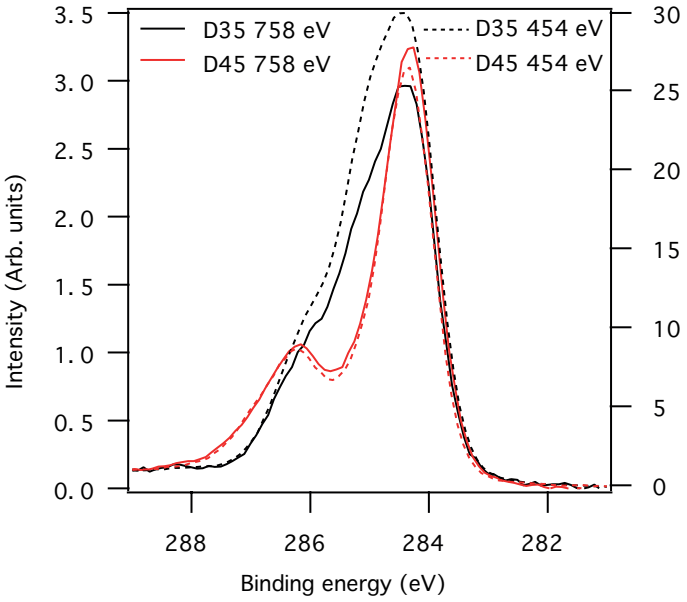

Fig. 9 Photon energy dependence in the C1s core-level photoelectron spectra. The dashed spectra are measured with a photon energy of 454 eV while the solid ones are measured with a photon energy of 758 eV. The dashed spectra thus provide higher surface sensitivity. All spectra are intensity normalized against the corresponding Ti2p (for 758 eV) or Ti3p (for 454 eV) signal.

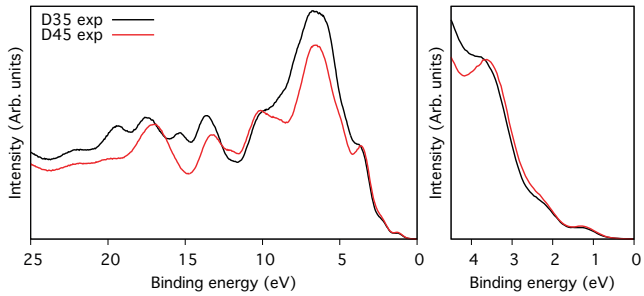

Fig. 10 The valence level spectra of D35 and D45. The small features at low binding energy are the HOMO levels of the dyes. The spectra are measured with a photon energy of 150 eV.

3.3 Energy level matching

Figure 10 shows the valence level spectra of D35 and D45 absorbed on a TiO_2 surface and measured with 150 eV photon energy. The larger features between 5 and 25 eV binding energy are mainly from the substrate and carbon signal (Ti, C, and O) forming molecular orbitals. The small peaks at roughly 1.5 eV are the highest occupied molecular orbitals (HOMO levels) from the dyes. As can be seen, D35 and D45 have similar binding energy of the HOMO levels, which is in accordance with electrochemical measurements[4,11].

The second set of DFT calculations concern the electronic structure and interpretation of the experimental photoelectron spectra and will be presented in this section. Valence photoelectron spectroscopy can be used to study the valence band and determine the character and density of the highest occupied states in the dyes. In Figure 11, the experimental valence spectra of D35 and D45

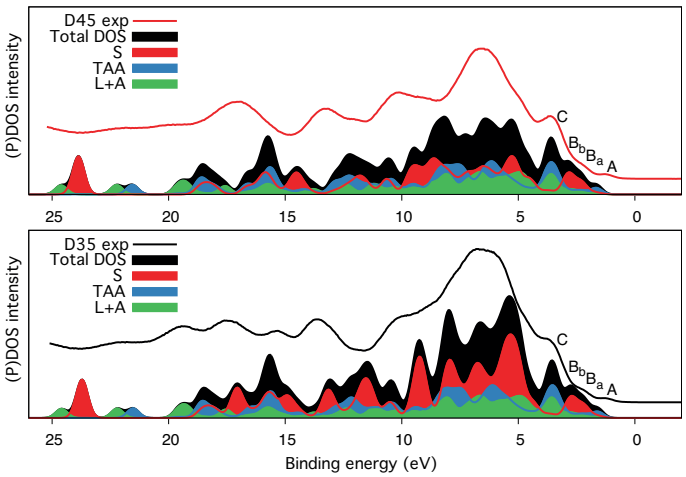

Fig. 11 The experimental valence levels (from Figure 10) compared to calculated density of states for D35 and D45. Partial density of states are shown from the unit including the alkoxy substituents (S), the triarylamine unit (TAA), and linker and anchor units (L+A). The hydrogen atoms were excluded in the calculations.

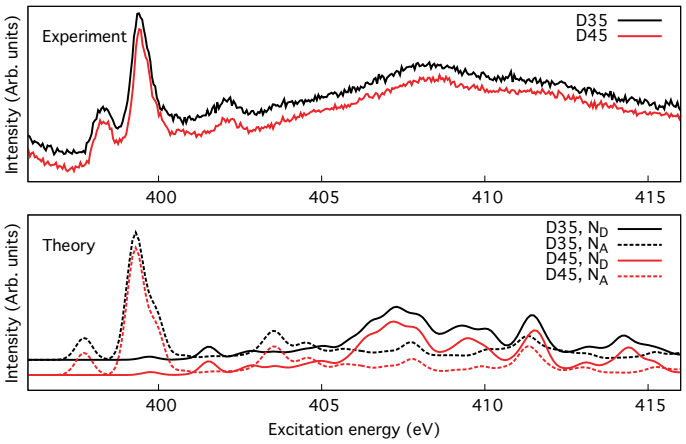

Fig. 12 Experimental and calculated nitrogen K-edge X-ray absorption spectra of D35 and D45. In the calculations the contributions from the cyano (acceptor) group denoted as N_A and the triarylamine group (donor) denoted as N_D are presented.

adsorbed to TiO_2 (from Figure 10) are compared to theoretical spectra of isolated dye molecules, with intact -COOH carboxyl groups. The theoretical spectra reproduce the overall spectral shape very well and can be used to reliably assign the low-binding energy features. However, for agreement with the experimental spectra in the whole energy range shown in Figure 11, the energy-scale from the calculations would have to be stretched to account for differential relaxation effects in the ionization process.

The states at low binding energy, denoted A–C in the D35 and D45 valence spectra in Figure 11, are similar for both dyes; the longer alkoxy chains in the D35 molecule thus mainly contribute to the valence orbitals corresponding to binding energies higher than 4 eV. The most important differences between the D35 and D45 valence spectra are observed in the region 4–10 eV, where the D45 intensity is lower, and in the region about 11.5–18 eV (10–15 eV in the theoretical spectrum).

We notice that for the photooxidation of the dye molecules by visible light, the highest occupied molecular orbitals (HOMOs) are important. Hence, in the photoemission spectra in Figure 11, we focus on the low binding energy peaks which we denote A, B_a, B_b, and C. The decomposition of the total DOS of the dye molecules into PDOS for the linker and acceptor units (L+A) and for the separate contributions from the triarylamine moiety (TAA), and the part of the donor unit containing the phenyl group with the alkoxy chains (S) shows that the HOMO is mainly localized on the donor (S and TAA units). In comparison to a previous electronic structure study of triarylamine based dyes,[47] we observe additional features in the outermost structure of the D35 and D45 valence PES spectra, arising from the π bonding orbitals on the S unit present in these dyes. These two peaks B_a and B_b are separated by 0.5 eV and are characterized by the orientation of the nodal plane of π bonding orbitals on the S unit phenyl group. The orbitals contributing to the peak denoted C are mostly localized on the TAA unit, with a large contribution also from the L and A units.

As seen in Figure 11, the difference in DOS can be attributed to the amount of carbon, but despite the significant change in molecular structure, we conclude from the experimental PES data and the spectrum calculations that the occupied valence band energy levels of D35 and D45 are similar. To probe also the unoccupied levels N1s, XAS measurements and calculations were performed. For both of the measured samples and also for calculations of the isolated molecules, the XAS of D35 and D45 are very similar as seen in the results presented in Figure 12. The most distinct difference is the feature at 401 eV only seen in D45, but the assignment against the calculations is not straight forward, since the calculations of D35 and D45 are nearly identical. Further studies on a well-defined experimental model system could determine if the feature at 401 eV contains information about interactions with the cyano group.

4 Conclusions

The surface coverage was found to be significantly higher for D45 than for D35. However, the solar cell performance is higher for solar cells with D35 and the differences in solar cell characteristics when longer alkoxy chains are introduced in the triarylamine unit are attributed to geometrical changes in the dye packing. The XPS data show that the butoxy chains are located close to the outermost surface and the longer butoxy chains in D35 therefore effectively protect the surface and suppress recombination with the redox couple and therefore give a longer electron lifetime in a dye-sensitized solar cell. The main conclusion from the theoretical calculations as well as from the PES studies is that the organic dyes D35 and D45 have strikingly similar electronic structure and that introducing the longer alkoxy chains does not affect the energy level matching. The differences in electron lifetimes can thus not be attributed to energy matching changes. Hence, the main conclusion from the present paper is that pure changes in geometrical configurations have vast consequences on the electron lifetime and are therefore responsible for the changes observed in solar cell performance. This is of importance for future dye design

and hence future striving for higher power conversion efficiencies of the DSC.

5 Acknowledgements

We acknowledge financial support from the Swedish Research Council, the Carl Trygger foundation, the Swedish Energy Agency and STandUP for Energy. The computations were partly performed on resources provided by the Swedish National Infrastructure for Computing (SNIC) at the Swedish National Supercomputer Center (NSC) and the High Performance Computer Center North (HPC2N). A. A. and S. F. thank MIUR-PRIN-2010 20104XET32 "DSSCX" for financial support. The kind and helpful staff at the MAX IV laboratory is greatly acknowledged.

References

1 B. O'Regan and M. Grätzel, *Nature*, 1991, **353**, 737–740.
2 A. Hagfeldt, G. Boschloo, L. Sun, L. Kloo and H. Pettersson, *Chem. Rev.*, 2010, **110**, 6595–6663.
3 D. P. Hagberg, T. Marinado, K. M. Karlsson, K. Nonomura, P. Qin, G. Boschloo, T. Brinck, A. Hagfeldt and L. Sun, *J. Org. Chem.*, 2007, **72**, 9550–9556.
4 D. P. Hagberg, X. Jiang, E. Gabrielsson, M. Linder, T. Marinado, T. Brinck, A. Hagfeldt and L. C. Sun, *J. Mater. Chem.*, 2009, **19**, 7232–7238.
5 A. Mishra, M. Fischer and P. Bäuerle, *Angew. Chem. Int. Ed.*, 2009, **48**, 2474–2499.
6 D. P. Hagberg, T. Edvinsson, T. Marinado, G. Boschloo, A. Hagfeldt and L. Sun, *Chem. Commun.*, 2006, 2245–2247.
7 L. Kloo, *Chem. Commun.*, 2013, **49**, 6580–6583.
8 S. M. Feldt, E. A. Gibson, E. Gabrielsson, L. Sun, G. Boschloo and A. Hagfeldt, *J. Am. Chem. Soc.*, 2010, **132**, 16714–16724.
9 H. Ellis, S. K. Eriksson, S. M. Feldt, E. Gabrielsson, P. W. Lohse, R. Lindblad, L. C. Sun, H. Rensmo, G. Boschloo and A. Hagfeldt, *J. Phys. Chem. C*, 2013, **117**, 21029–21036.
10 T. N. Murakami, N. Koumura, M. Kimura and S. Mori, *Langmuir*, 2014, **30**, 2274–2279.
11 H. Tian, E. Gabrielsson, P. W. Lohse, N. Vlachopoulos, L. Kloo, A. Hagfeldt and L. Sun, *Energy Environ. Sci.*, 2012, **5**, 9752–9755.
12 K. Westermark, S. Tingry, P. Persson, H. Rensmo, S. Lunell, A. Hagfeldt and H. Siegbahn, *J. Phys. Chem. B*, 2001, **105**, 7182–7187.
13 J. Nyhlen, G. Boschloo, A. Hagfeldt, L. Kloo and T. Privalov, *ChemPhysChem*, 2010, **11**, 1858–1862.
14 M. Bassler, J. O. Forsell, O. Björneholm, R. Feifel, M. Jurvansuu, S. Aksela, S. Sundin, S. L. Sorensen, R. Nyholm, A. Ausmees and S. Svensson, *J. Electron. Spectrosc. Relat. Phenom.*, 1999, **101**, 953–957.
15 E. M. J. Johansson, M. Hedlund, H. Siegbahn and H. Rensmo, *J. Phys. Chem. C*, 2005, **109**, 22256–22263.
16 E. M. J. Johansson, T. Edvinsson, M. Odelius, D. P. Hagberg, L. H. Sun, A. Hagfeldt, H. Siegbahn and H. Rensmo, *J. Phys. Chem. C*, 2007, **111**, 8580–8586.
17 F. De Angelis, S. Fantacci, A. Selloni, M. K. Nazeeruddin and M. Grätzel, *J. Phys. Chem. C*, 2010, **114**, 6054–6061.
18 M. Pastore, S. Fantacci and F. De Angelis, *J. Phys. Chem. C*, 2013, **117**, 3685–3700.
19 C. Anselmi, E. Mosconi, M. Pastore, E. Ronca and F. De Angelis, *Phys. Chem. Chem. Phys.*, 2012, **14**, 15963–15974.
20 M. Pastore and F. De Angelis, *J. Phys. Chem. Lett.*, 2013, **4**, 956–974.
21 M. Pastore and F. De Angelis, *Phys. Chem. Chem. Phys.*, 2012, **14**, 920–928.
22 J. Calbo, M. Pastore, E. Mosconi, E. Orti and F. De Angelis, *Phys. Chem. Chem. Phys.*, 2014, **16**, 4709–4719.
23 M. Pastore and F. De Angelis, *Top. Curr. Chem.*, 2014, **352**, 151–236.
24 G. te Velde, F. Bickelhaupt, E. Baerends, C. Guerra, S. Van Gisbergen, J. Snijders and T. Ziegler, *J. Comput. Chem.*, 2001, **22**, 931–967.
25 C. Guerra, J. Snijders, G. te Velde and E. Baerends, *Theor. Chem. Acc.*, 1998, **99**, 391–403.
26 J. Perdew, K. Burke and M. Ernzerhof, *Phys. Rev. Lett.*, 1996, **77**, 3865–3868.
27 S. Grimme, *J. Comput. Chem.*, 2006, **27**, 1787–1799.
28 E. Van Lenthe and E. Baerends, *J. Comput. Chem.*, 2003, **24**, 1142–1156.
29 A. Klamt, *J. Phys. Chem.*, 1995, **99**, 2224–2235.
30 A. Klamt and G. Schuurmann, *J. Chem. Soc., Perkin Trans. 2*, 1993, 799–805.
31 A. Klamt and V. Jonas, *J. Chem. Phys.*, 1996, **105**, 9972–9981.
32 C. Pye and T. Ziegler, *Theo*, 1999, **101**, 396–408.
33 StoBe-deMon version 3.2 (2013), K. Hermann and L.G.M. Pettersson, M.E. Casida, C. Daul, A. Goursot, A. Koester, E. Proynov, A. St-Amant, and D.R. Salahub. Contributing authors: V. Carravetta, H. Duarte, C. Friedrich, N. Godbout, J. Guan, C. Jamorski, M. Leboeuf, M. Leetmaa, M. Nyberg, S. Patchkovskii, L. Pedocchi, F. Sim, L. Triguero, and A. Vela.
34 A. D. Becke, *Phys. Rev. A*, 1988, **38**, 3098–3100.
35 J. P. Perdew, *Phys. Rev. B*, 1986, **34**, 7406–7406.
36 N. Godbout, D. R. Salahub, J. Andzelm and E. Wimmer, *Can. J. Chem.*, 1992, **70**, 560–571.
37 L. Triguero, L. G. M. Pettersson and H. Ågren, *Phys. Rev. B*, 1998, **58**, 8097–8110.
38 W. Kutzelnigg, U. Fleischer and S. M., *NMR-Basic Principles and Progress*, Springer Verlag, Heidelberg, 1990.
39 L. G. M. Pettersson, U. Wahlgren and O. Gropen, *Chem. Phys.*, 1983, **80**, 7–16.
40 L. G. M. Pettersson, U. Wahlgren and O. Gropen, *J. Chem. Phys.*, 1987, **86**, 2176–2184.
41 H. Ågren, V. Carravetta, O. Vahtras and L. G. M. Pettersson, *Theor. Chem. Acc.*, 1997, **97**, 14–40.
42 J. Guan, P. Duffy, J. T. Carter, D. P. Chong, K. C. Casida, M. E. Casida and M. Wrinn, *J. Chem. Phys.*, 1993, **98**, 4753–4765.
43 E. Ronca, M. Pastore, L. Belpassi, F. Tarantelli and F. De Angelis, *Energy Environ. Sci.*, 2013, **6**, 183–193.
44 H. Ellis, I. Schmidt, A. Hagfeldt, G. Wittstock and

G. Boschloo, *J. Phys. Chem. C*, 2015, **Article ASAP**, DOI: 10.1021/acs.jpcc.5b04436.
45 P. J. Cumpson, *Surf. Interface Anal.*, 2001, **31**, 23–34.
46 M. Hahlin, E. M. J. Johansson, S. Plogmaker, M. Odelius, D. P. Hagberg, L. C. Sun, H. Siegbahn and H. Rensmo, *Phys. Chem. Chem. Phys.*, 2010, **12**, 1507–1517.
47 M. Hahlin, M. Odelius, M. Magnuson, E. M. J. Johansson, S. Plogmaker, D. P. Hagberg, L. C. Sun, H. Siegbahn and H. Rensmo, *Phys. Chem. Chem. Phys.*, 2011, **13**, 3534–3546.